THE JOURNAL OF PHYSICAL CHEMISTRY B

pubs.acs.org/JPCB

Article

Morphology Modulation of Ionic Surfactant Micelles in Ternary Deep Eutectic Solvents

Published as part of The Journal of Physical Chemistry virtual special issue "Deep Eutectic Solvents".

Ria S. Atri, Adrian Sanchez-Fernandez, Oliver S. Hammond, Iva Manasi, James Doutch, James P. Tellam, and Karen J. Edler*

Cite This: *J. Phys. Chem. B* 2020, 124, 6004–6014

Read Online

ACCESS | Metrics & More | Article Recommendations | Supporting Information

ABSTRACT: Deep eutectic solvents (DES) are potentially greener solvents obtained through the complexation of simple precursors which, among other applications, have been investigated in recent years for their ability to support the self-assembly of amphiphilic molecules. It is crucial to understand the factors which influence surfactant solubility and self-assembly with respect to the interaction of the surfactant molecule with the DES components. In this work, small-angle neutron scattering (SANS) has been used to investigate the micellization of cationic (C_nTAB) and anionic (SDS) surfactants in a ternary DES comprising choline chloride, urea, and glycerol, where the hydrogen bond donors are mixed in varying molar ratios. The results show that in each case either globular or rodlike micelles are formed with the degree of elongation being directly dependent on the composition of the DES. It is hypothesized that this composition dependence arises largely from the poor solubility of the counterions in the DES, especially at low glycerol content, leading to a tighter binding of the counterion to the micelle surface and giving rise to micelles with a high aspect ratio. This potential for accurate control over micelle morphology presents unique opportunities for rheology control or to develop templated syntheses of porous materials in DES, utilizing the solvent composition to tailor micelle shape and size, and hence the pore structure of the resulting material.

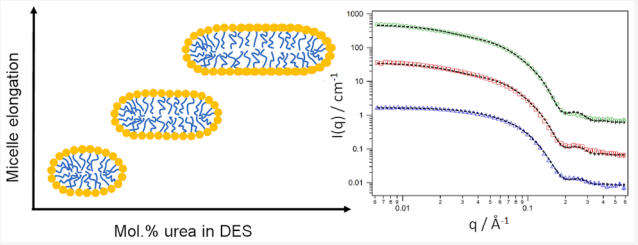

INTRODUCTION

Amphiphile self-assembly in ionic liquids (ILs) was first demonstrated in 1982 for ethylammonium nitrate,[1] and well over 30 protic ionic liquids are now known to exhibit this behavior.[2] Applications involving these systems range from polymers and polymer membranes[3−5] to the synthesis of porous materials.[6,7] Although ionic liquids possess several advantages such as low vapor pressure, low flammability, and a wide liquid range,[8] they may also present high expense, synthetic challenges, and non-negligible toxicity which may prevent their widespread use in industry.[9]

Deep eutectic solvents (DES) are often considered to be analogues of room-temperature ionic liquids (RTILs), except that they contain a significant molecular component. While DES share several common properties with ILs, they can be easier to prepare and often comprise relatively cheap, widely available, and environmentally benign components.[10] DES have found application in a wide range of research fields including organic synthesis and transformations,[11,12] inorganic synthesis,[13−15] separations and extractions,[16,17] and electrochemistry.[18−20]

More recently, the ability of DES to support self-assembly has been demonstrated. For example, in choline chloride/urea, phospholipids solubilize with minimal water content, causing them to spontaneously self-assemble into lamellar phases which transform to vesicles over time.[21] Uniquely, the stability of the bilayer phase depends upon the nanostructure of the DES itself, which is not the case for molecular solvents.[22] DES have also been found to stabilize large-scale structures, such as polymers,[23−25] proteins,[26,27] and dye molecule aggregates.[28,29]

Our recent work has demonstrated the capability of DES to solubilize both cationic and anionic surfactants, and we have carried out numerous studies combining tensiometry, neutron and X-ray reflectivity and scattering techniques to characterize micelle morphology and surfactant-DES interactions.[30−32] It has become apparent that DES composition has a marked effect on the solubility of amphiphilic molecules: for example, cationic alkyltrimethylammonium bromide (C_nTAB) surfactants are insoluble in choline chloride/urea, whereas the anionic sodium dodecyl sulfate (SDS) is soluble up to relatively high concentrations.[30,31] For surfactant/ionic liquid

Received: April 30, 2020
Revised: June 14, 2020
Published: June 17, 2020

https://dx.doi.org/10.1021/acs.jpcb.0c03876
J. Phys. Chem. B 2020, 124, 6004–6014

solutions, it has been shown that a surfactant−solvent counterion exchange can occur in the system, where surfactant counterions are incorporated into the bulk solvent, while ions in the solvent interact with the micelle surface.[33] As has been observed for aqueous systems,[34] the morphology of micelles in DES is strongly dependent upon the interaction of the surfactant headgroup and counterion with the solvent. For SDS, Coulombic interactions between the DES $[cholinium]^+$ with the surfactant SO_4^- headgroups provide a charge screening effect which allows for the headgroups to pack more closely and causes micelle elongation.[35] This observation also explains the tendency of cationic C_nTAB surfactants to form spheroidal rather than elongated micelles in choline-based solvents, due to the presence of chloride and bromide ions within the DES which interact with the positively charged headgroups. Neither of these ions cause significant changes in the micelle shape for C_nTAB micelles in water until extremely high concentrations are reached.[36]

Surfactant micelles have been used as templating agents in the synthesis of various porous materials. Examples of this include the synthesis of mesoporous materials including silica[37,38] and metal oxides.[39] Recently, Chen et al. reported the surfactant template-assisted synthesis of hierarchical ZIF-8 particles using sodium dodecyl sulfate (SDS) in choline chloride/urea.[40] This method allowed for porosity in the product to be tuned directly by variation of the amount of SDS and water in the reaction mixture. In our previous work,[41] we have synthesized iron oxide nanoparticles via a simple solvothermal process using the choline chloride/urea solvent, with the morphology of the products controlled by the water content of the reaction mixture. Furthermore, we have shown that the urea component of the DES is crucial to the solvothermal reaction mechanism.

While SDS readily forms micelles in the choline chloride/urea DES, C_nTAB surfactants are insoluble in this system. In choline chloride/glycerol, the cationic surfactants readily assemble to form ellipsoidal micelles, with the tail length directly affecting the degree of elongation the micelles display;[31] behavior which is similar to their self-assembled aggregates in water. In order to both support the micellization of cationic and anionic surfactant molecules and retain the urea functionality (which is essential to the solvothermal reaction mechanism creating inorganic oxide particles), as well as to explore the effect of urea content on solubility and self-assembly, we have used a three-component deep eutectic system comprising choline chloride, urea and glycerol in varying urea/glycerol ratios. Such a system has been briefly characterized by Kadhom et al.,[42] but not put to any application. The behavior of cationic C_nTAB surfactants and the anionic SDS in this ternary DES have been studied using small-angle neutron scattering (SANS) techniques. Understanding how the morphology of the obtained micelles can be related to the urea/glycerol ratio in the DES will provide a method to selectively tune the structure of the micelles and any micelle-templated materials grown in such solvents through careful control of the DES composition.

EXPERIMENTAL SECTION

Materials. Choline chloride (h-ChCl, ≥98%), urea (h-U, ≥99.5%), and glycerol (h-Gly, ≥99.5%) were all purchased from Sigma-Aldrich. The deuterated materials ChCl-d_9 (d-ChCl, 99% atom, 99.9% D), urea-d_4 (d-U, 99% atom, 98% D), and glycerol-d_8 (d-Gly, 99% atom, 99% D) were purchased from Cambridge Isotope Laboratories. For simplicity, we refer to a "fully deuterated solvent" throughout this work as that which is prepared using deuterated precursors (d-ChCl/d-U/d-Gly), although the d-ChCl component is actually the partially deuterated compound $(CD_3)_3NC_2H_4OHCl$.

Dodecyltrimethylammonium bromide (C_{12}TAB, ≥99%), hexadecyltrimethylammonium bromide (C_{16}TAB, ≥99%), and sodium dodecyl sulfate (SDS ≥ 99%) were purchased from Sigma-Aldrich. Isotopically labeled surfactants consisting of deuterated head and tail components (C_{16}TAB-d_{42} and C_{12}TAB-d_{34}) or with selective deuteration of the tail (C_{16}TAB-d_{33}, C_{12}TAB-d_{25}, and SDS-d_{25}) were supplied by the STFC ISIS Deuteration Facility. Due to the hygroscopic nature of choline chloride, both h-ChCl and d-ChCl were dried under vacuum at 80 °C for at least 12 h immediately prior to use in order to minimize water content in the resultant DES. All other chemicals were used as received without further purification.

Solvent and Sample Preparation. The ternary choline chloride/urea/glycerol (ChCl/U/Gly) DES was prepared by combining the three components in molar ratios of ChCl/U/Gly = 1:1.5:0.5, 1:1:1, and 1:0.5:1.5. These mixtures were stirred at 60 °C until a clear, homogeneous liquid was obtained, which was subsequently sealed and equilibrated at 40 °C overnight. Once formed, the mixtures are stable in the liquid state at room temperature.

Surfactant in DES solutions containing SDS were mixed and equilibrated at 40 °C until a homogeneous mixture was obtained, while for solutions containing C_{12}TAB and C_{16}TAB, it was necessary to prepare mixtures at 60 °C due to their high Krafft points in the DES.

DES Characterization. The densities of the solvents were determined from a triplicate average of measurements on an Anton Paar DMA 4500 M at 25 °C. The surface tension of the neat solvents was measured using an Attension Sigma 700 force tensiometer, using the du Noüy ring method.

Differential scanning calorimetry (DSC) measurements on the neat solvents were carried out on a TA Instruments DSC-Q20 differential scanning calorimeter. The sample was first equilibrated at 50 °C and held for 1 min, cooled to −75 °C at a ramp rate of 10 °C min^{-1} and held for 10 min, before heating to 30 °C at a ramp rate of 5 °C min^{-1}.

The viscosity of the solvents was measured using a TA Instruments HR-3 Discovery Hybrid Rheometer operating in flat plate geometry with Peltier temperature control. Viscosity data was obtained in a temperature range of 20−85 °C. The DES were measured as prepared, with a seal of mineral oil to prevent solvent interaction with the atmosphere during measurements. Although Kadhom et al.[42] suggested a non-Newtonian behavior for these solvents at low temperatures, we did not observe this in the measured temperature range of our experiments and therefore data were collected at a fixed shear rate of 1 s^{-1}.

The solubility of sodium bromide, NaBr, in the DES was estimated by gradual addition of known amounts of salt to the DES with continuous stirring at 25 °C.

DSC and viscosity data are presented in the Supporting Information. Results from density, surface tension, and solubility measurements are included in Table 1.

Small-Angle Neutron Scattering. Small-angle neutron scattering (SANS) measurements were carried out on the LOQ,[43] and ZOOM instruments at ISIS Pulsed Neutron and Muon Source, UK. LOQ is a fixed-geometry time-of-flight instrument with two detectors positioned at 0.5 and 4 m from

https://dx.doi.org/10.1021/acs.jpcb.0c03876
J. Phys. Chem. B 2020, 124, 6004−6014

the sample, utilizing neutron wavelengths between 2.2 and 10 Å to provide a Q-range of 0.008−1.6 $Å^{-1}$. ZOOM is a time-of-flight instrument capable of accessing a Q-range of 0.0045−0.85 $Å^{-1}$ when operating with a sample-to-detector distance of 4 m.

For both experiments, samples were sealed in 1 mm path length quartz cuvettes (Hellma GmbH) and loaded onto an automatic sample changer. A single measurement temperature of 70 °C was chosen, first in order to remain above the Krafft temperature of the cationic surfactant mixtures and second because this was closer to the reaction temperature for a templated synthesis while remaining below the degradation threshold for urea, which is ca. 80 °C in the DES.[44]

Data reduction was performed following the standard procedures on each instrument using the routines within Mantid.[45] The data were normalized to the sample transmission, calibrated to absolute units using a polymer standard, and corrected for detector efficiencies, before scattering from the empty cell was subtracted. The resulting output was converted to absolute units of the scattering intensity ($I(q)$, cm^{-1}) versus the momentum transfer (q, $Å^{-1}$). Subtraction of the scattering from the pure solvents was performed afterward using Igor Pro[46] to account for the incoherent contribution to each sample.

Surfactant mixtures in DES were prepared at concentrations of 25 and 130 mM in different isotopic mixtures to aid in resolving the micelle structure. Deuterated surfactant in h-ChCl/h-U/h-Gly and protiated surfactant in d-ChCl/d-U/d-Gly provided information on the size of the micelle core, as the scattering is dominated by the micelle core−solvent scattering length density correlation.

Data Analysis. Initially, the Guinier approximation was used to examine the low-q data and analyze the density distribution of the longest dimension of the scatterer and hence examine how micelle elongation varied with DES composition. This analysis allows the determination of the radius of gyration, R_g, of the scatterer, which, in scattering data analysis, quantifies the scattering length density (SLD) distribution of an object from its center of mass. At low volume fractions where colloidal interactions are negligible, an approximate size of the scatterers may be calculated by analyzing the low-q region of the data from a plot of $\ln(I)$ versus q^2.[47] The radius of gyration may then be calculated from the gradient of the resultant graph:

$$\ln(I(q)) = \ln(I(0)) - \frac{R_g^2}{3}q^2$$

A systematic, model-based approach was then applied to fit all SANS data. The scattered intensity, $I(q)$, of a system of monodisperse, isotropic, and centrosymmetric particles may be described by the equation:

$$I(q) = N\ V^2\ (\Delta\rho)^2\ P(q)\ S(q)$$

where N and V are the number of particles and the volume of the particles, respectively. $\Delta\rho$ is the difference between the SLD of the scatterer and the solvent. $P(q)$ refers to the form factor, which describes scattering within the particle and therefore relates to the particle shape, and $S(q)$ is the structure factor, which describes the interaction between particles in the system. Although the structure factor may be considered to be negligible at low concentrations of scatterers, at higher concentrations it is important to account for interparticle interactions, which affect, in particular, the apparent scattered intensity at low q values.

We explored a range of geometric models in order to find a suitable fit for our data. These include a sphere model, cylindrical models (cylinder and core−shell cylinder), and ellipsoidal models (uniform and core−shell ellipsoid).[48] Details of each fit as applied to a 130 mM mixture of deuterated C_{16}TAB-d_{42} in protonated DES (urea/glycerol ratio of 1.5:0.5) may be found in Figure S3.

Although the sphere model appropriately fitted the data from globular micelles and the cylinder model appeared suitable for elongated micelles, an ellipsoidal model was ultimately chosen to fit all of the data as it covers a wide range of aspect ratios and appropriately describes the scattering from micelles presented in this work. This is also consistent with the results of previous investigations on similar systems.[31] This model contains structural parameters for the equatorial (r_{eq}) and polar (r_{po}) radii, where the equatorial dimension is the radius of the micelle through the rotational axis of the spheroid (see Figure S4 for a diagram). As such, it allows for an estimation of the cross-sectional size and degree of elongation of the micelle.

Furthermore, surfactant self-assembly in DES has been shown to result in the formation of micelles with a core−shell density distribution, where the surfactant tails remain at the core of the aggregate surrounded by a shell of solvated headgroups.[31,35] A uniform prolate ellipsoid model was initially used to fit the overall shape of the micelle. Subsequently, a core−shell ellipsoid model was used to determine the characteristics of the cross-sectional area of the micelle for those data sets which were sufficiently constrained. The SLD of the shell was fitted to account for the penetration of solvent, and the tail SLD was fixed, as it is considered that the penetration of the solvent into this solvophobic region is minimal.

The Percus−Yevick hard sphere structure factor[49] was used to account for the structure factor contribution to the scattering, as employed in previous work. This allows for the intermicellar interactions between the micelles which are evident in the data to be accounted for. The hard sphere structure factor comprises two parameters, the effective radius, r_{eff}, and effective volume fraction, $\Phi_{S(q)}$. The effective radius was calculated as the radius of a sphere with the same second virial coefficient as the scatterer, using the equation $r_{eff} = (r_{po}r_{eq}^2)^{1/3}$. $\Phi_{S(q)}$, which was not constrained to the form factor volume fraction, $\Phi_{P(q)}$, was determined through fitting. Such an approach has previously been used to account for the excess interactions which were attributed to short-range electrostatic repulsion occurring between charged micelles in DES and which could not be fitted using the standard excluded volume interaction potential.[50] This method provides a descriptive approach to fit the scattering from surfactant micelles in DES; however, direct physical interpretation of the results from the structure factor cannot be performed.

The SLD of each component in the system (solvent, surfactant headgroup, and tail) was calculated from the scattering length of the molecular assembly and the molecular volume they occupy. The molecular volumes of the solvents were calculated from the physical density measured at 25 °C. The calculated SLD values for each DES are given in Table S2, while the molecular volumes of the various groups, neutron scattering lengths, and their calculated SLDs are included in Table S3.

https://dx.doi.org/10.1021/acs.jpcb.0c03876
J. Phys. Chem. B 2020, 124, 6004−6014

Table 1. Solvent Properties for the Three DES Investigated in This Work Compared to Literature Values for Relevant Species

DES	density at 25 °C/g cm^{-3}	average molar mass/g mol^{-1}	M_v/ cm^3 mol^{-1}[b]	surface tension (γ)/mN m^{-1}	Gordon parameter (G)/J m^{-3}[c]	viscosity at 25 °C/Pa s	solubility of NaBr at 25 °C/g kg^{-1}
water	0.997	18.02	18.0	71.99[55]	2.743−2.750[2]	8.9 × 10^{-4} [56]	943.2[57]
1:2 ChCl/ urea[30]	1.15	86.6[a]	75.3	66 ± 1	1.57 ± 0.02	1.57[58]	
1:1.5:0.5 ChCl/ U/Gly	1.1970 ± 0.0001	91.9[a]	76.8	69.3 ± 0.7	1.63 ± 0.02	0.70 ± 0.2	50 ± 2
1:1:1 ChCl/U/ Gly	1.1957 ± 0.0003	97.3[a]	81.3	70.1 ± 0.6	1.62 ± 0.01	0.56 ± 0.1	58 ± 3
1:0.5:1.5 ChCl/ U/Gly	1.1945 ± 0.0001	102.6[a]	85.9	68.2 ± 0.5	1.55 ± 0.01	0.46 ± 0.1	65 ± 3
1:2 ChCl/ glycerol	1.19[59,60]	107.9[a]	90.7	63.5 ± 0.5[31]	1.41 ± 0.01	0.26[61]	
glycerol	1.26[56]	92.1	73.1	62.5[62−64]	1.51[63]	0.91[64]	387[65]

[a]Calculated as the average molar mass by considering the ratio of components in each DES. [b]Molar volumes were calculated by considering the density and average molar mass of each sample. [c]Gordon parameters were calculated from surface tension measurements.

RESULTS AND DISCUSSION

Solvent Composition and Physical Properties. Table 1 shows the densities, average molar masses, molar volumes, surface tensions, calculated Gordon parameter, and solubilities of NaBr in the DES investigated in this work. Where possible, data for water, ChCl/urea, ChCl/glycerol, and glycerol are presented for comparison. Molar volumes for the ternary DES were calculated using their measured densities and average molar masses. The Gordon parameter,[51] G, may be calculated from surface tension data using the following equation:

$$G = \frac{\gamma}{V_m^{1/3}}$$

This parameter is a description of the "solvophobicity" of a solvent and is comparable to quantifying the hydrophobic effect in water.[52] It provides a measure of the cohesiveness of solvent molecules and may therefore be used to predict the capability of a solvent to promote the self-assembly of amphiphilic molecules.[53,54]

The ternary DES all have slightly higher surface tensions than those of the binary ChCl/urea and ChCl/glycerol DES. Although small differences between these may arise from the use of different techniques (du Noüy ring or pendant drop method), the results presented here allow a direct comparison of the surface tension values of the ternary DES. It is interesting to note that, in a similar system, upon the addition of 1 mol equiv of water, the surface tension of 1:1 choline chloride/malic acid also increases by 12 mN m^{-1}, from 65 to 77 mN m^{-1}, while the addition of 2 mol equiv of water does not further alter the surface tension.[66] This increase in surface tension upon water addition was attributed to changes in the H-bond network and the concomitant effect on solvent cohesivity. While this change in surface tension could also be due to a saturation of species at the DES surface, this is unlikely both due to the comparatively low water content in the DES and the strong interactions of water molecules with the DES components. Water molecules are not expected to preferentially assemble at the air−liquid interface, causing an increase in the surface tension. A surface excess of the other species would not change the observed surface tension compared to the dry DES, as the interface would still be made up of the mixed DES components. Therefore, we suggest that the addition of a third hydrogen bond donor to the DES (e.g., glycerol to ChCl/urea) may result in a rearrangement of the solvent structure allowing formation of a greater number of H-bonds than in the relatively constrained binary systems. As such, the resulting structure may be more cohesive and therefore show a higher surface tension at the interface. However, after initial glycerol addition the surface tensions appear to rapidly saturate, and there is little variation between values for the three ternary DES, although all values are below the surface tension of water and higher than that of glycerol.

Due to the differences in molar volumes, the values of the Gordon parameter calculated from the surface tension values show a small decreasing trend with added glycerol content. These values are however still similar across all investigated systems, and it may be assumed that they contain comparable hydrogen-bonding interactions. As such, any observed differences in micelle morphology cannot be attributed to a variation in hydrogen bonding across solvent compositions.

The same is also true for the measured density values, which vary little with composition. Interestingly, while ChCl/glycerol has a lower viscosity than pure glycerol, the addition of urea increases the viscosity of the ternary systems. The DES with the highest urea content also has the highest viscosity at low temperature. In all cases, the data could be fitted as following an exponential decay as per the Arrhenius equation (with R^2 values > 0.99). At higher temperatures (above 50 °C), the viscosity values of all three DES become very similar. At the experimental temperature of 70 °C, the difference in viscosities is negligible and therefore cannot influence self-assembly as surfactant species will be equally free to move within these DES to find thermodynamically favored structures.

Solvent Composition and Micelle Morphology at Low Surfactant Concentration. As described above, the Guinier approximation was initially used to analyze the low-q region of the data, to estimate the elongation of the micelles in the low concentration solutions (25 mM). Previous studies on surfactant behavior in DES have shown that at similarly low concentrations the intermicellar interactions are negligible; therefore, the scattering curve depicts the form factor of the micelles.[31,35] Micelle formation was not observed in the mixtures containing 25 mM C_{12}TAB as this concentration is probably close to the CMC of the surfactant. Instead, R_g results were obtained from the model-based analysis of 130 mM of C_{12}TAB. It is expected that this will still allow for a comparison of values of R_g as it has previously been demonstrated that micelle morphology for mixtures of C_{12}TAB in DES is not greatly affected by concentration.[31] The Guinier fits (plotted as $\log(I(q))$ vs $\log(q)$) and the R_g results for the surfactants in different solvents are shown in Figure 1 and Figure 2,

https://dx.doi.org/10.1021/acs.jpcb.0c03876
J. Phys. Chem. B 2020, 124, 6004−6014

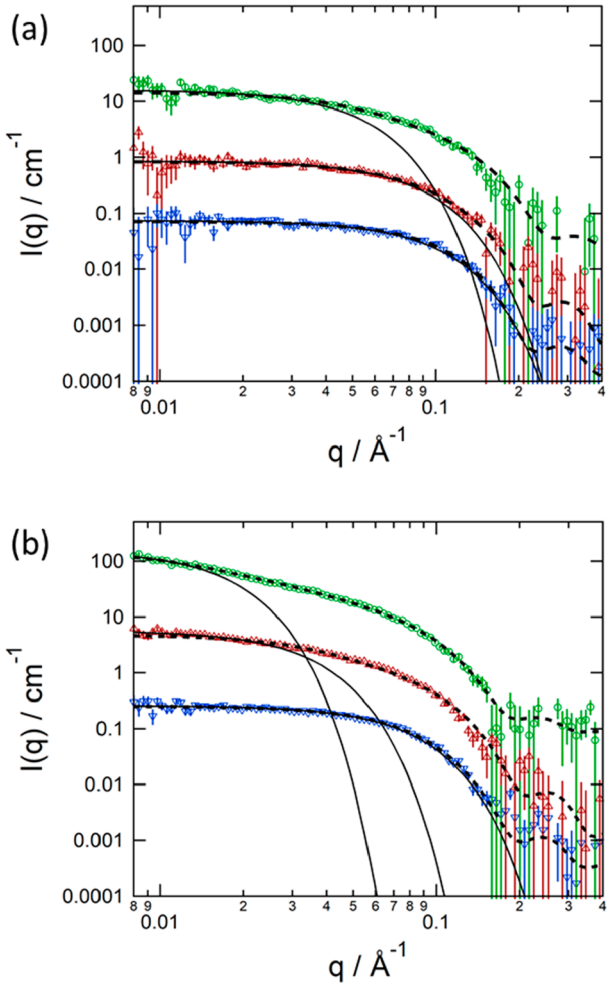

Figure 1. SANS data and best fits of 25 mM solutions of SDS-d_{25} (a) and C_{16}TAB-d_{42} (b) in 1:1.5:0.5 (green circles), 1:1:1 (red upward triangles), and 1:0.5:1.5 (blue downward triangles) h-ChCl/h-U/h-Gly. The fits correspond to the Guinier analysis at low q (solid lines) and model-based analysis using a uniform ellipsoid model (dashed lines).

respectively. The R_g values for those micelles in ChCl/urea (1:2:0) and ChCl/glycerol (1:0:2) are presented for comparison. A full record of the fitted parameters may be found in the Supporting Information.

It has previously been shown that dodecyl sulfate surfactants form larger micelles in ChCl/U than in ChCl/Gly.[32] Additionally, SDS micelles in ChCl/Gly are of similar dimensions to those of C_{12}TAB surfactants in the same solvent, with aspect ratios (r_{po}/r_{eq}) below 2.[31] This change in micelle elongation with increasing glycerol content in the solvent is also observed here in the scattering data, where the low-q Guinier region shifts continuously to higher momentum transfers related to smaller scatterers. Following this trend, it is observed that micelles become more elongated as the urea content of the ternary DES increases. For each solvent, the largest assemblies are obtained for C_{16}TAB, followed by SDS, and the least elongated micelles are of C_{12}TAB. In each case, the micelles in DES were larger than those in water ($R_{g,SDS} \sim 16$ Å, $R_{g,C_{12}TAB} = 16.8$ Å, $R_{g,C_{16}TAB} = 25.4$ Å), where these surfactants form globular, strongly interacting micelles at these concentrations.[31,67] This has been previously attributed to the stronger cohesive forces of water and to the partial charge neutralization provided by the ions present in the DES.[35] It is also interesting to note that C_{12}TAB and C_{16}TAB form micelles in all of the ternary DES, even at high a concentration of urea in the solvent (1:1.5:0.5), in contrast with the extremely low solubility of those surfactants in ChCl/U, where no micellar assembly was observed.[30] As such, it has been demonstrated that the presence of glycerol assists surfactant solubility, and so the formation of micelles even at relatively low glycerol concentration.

Considering the behavior of dodecyl sulfate surfactants in 1:2 ChCl/U and 1:2 ChCl/Gly,[32] it was initially hypothesized that the elongation of the micelles would vary with solvent composition, with a higher glycerol content in the DES reducing elongation. The trend observed from these initial fits indicates that this is indeed the case, where an increase in the glycerol concentration results in the formation of smaller micelles.

The model-based analysis performed using the uniform ellipsoid model shows that the elongation of the micelles (r_{po}) varies greatly with changing glycerol content in the solvent,

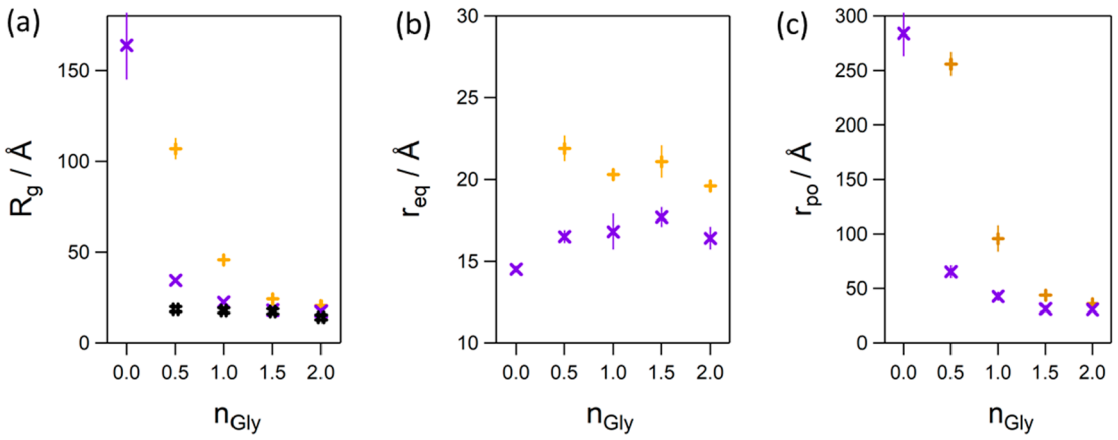

Figure 2. Structural parameters of surfactant micelles at different solvent compositions obtained through the Guinier analysis (a) R_g and uniform ellipsoid modeling (b) r_{eq}, and (c) r_{po}. The data is labeled as the following: SDS (purple crosses), C_{12}TAB (black hash marks), and C_{16}TAB (yellow crosses). Error bars are the result of averaging the values obtained from fits to the data of multiple contrasts of the same mixture.

https://dx.doi.org/10.1021/acs.jpcb.0c03876
J. Phys. Chem. B 2020, 124, 6004−6014

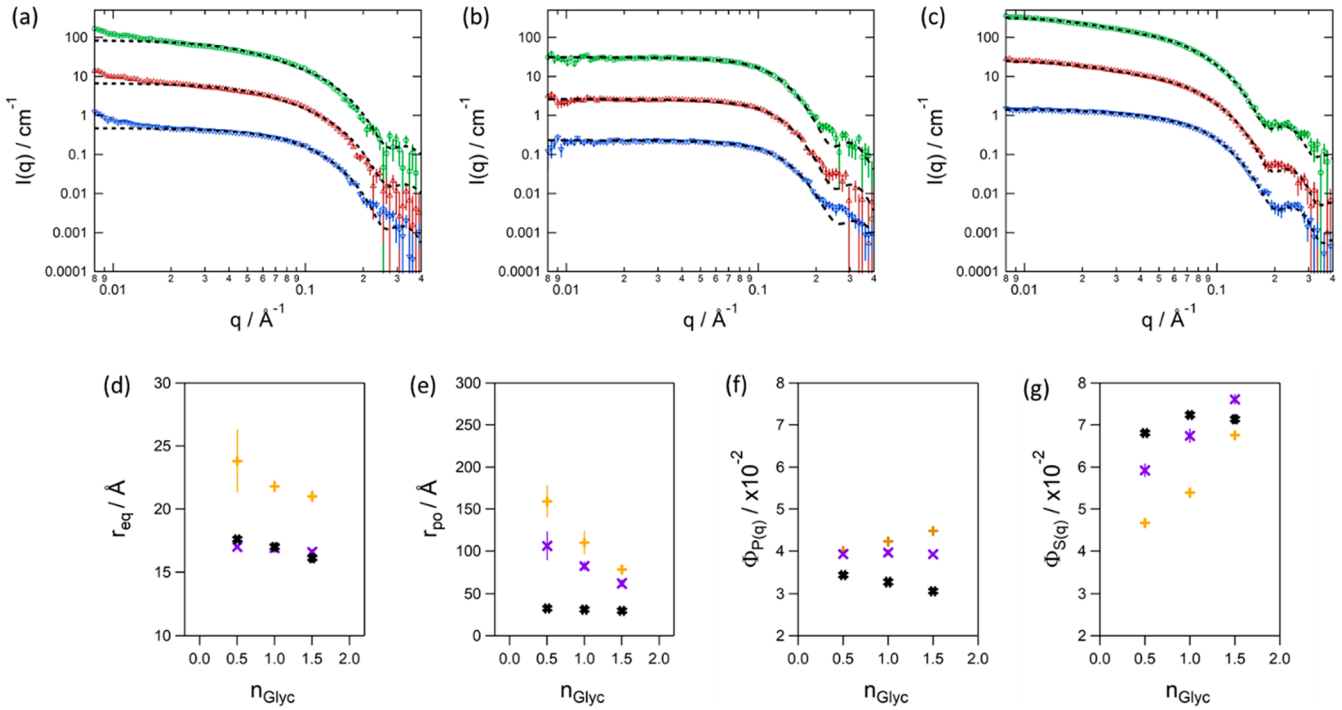

Figure 3. (Top) SANS data and best fits of 130 mM of SDS-d_{25} (a), C_{12}TAB d_{34} (b), and C_{16}TAB-d_{42} (c) in 1:1.5:0.5 (green circles), 1:1:1 (red upward triangles) and 1:0.5:1.5 (blue downward triangles) h-ChCl/h-U/h-Gly. The dashed lines show the best fits obtained through corefinement of different contrasts to a uniform ellipsoid model including, where appropriate, a hard-sphere structure factor. (Bottom) Structural parameters of surfactant micelles at different solvent compositions obtained through model-based analysis (d) r_{eq}; (e) r_{po}; (f) $\Phi_{P(q)}$; (g) $\Phi_{S(q)}$): SDS (purple crosses), C_{12}TAB (black hash marks), and C_{16}TAB (yellow crosses).

while their cross sections (r_{eq}) remain largely unchanged for each surfactant. The r_{eq} of SDS micelles is of similar dimensions to those observed in other DES and smaller than that of C_{16}TAB, which is as expected since the solvophobic moiety of the former is larger than that of SDS.[31,35] At low glycerol content, primarily at 1:1.5:0.5 ChCl/U/Gly, SDS and C_{16}TAB form elongated micelles and this elongation decreases as the amount of glycerol in the solvent is increased but in a nonlinear fashion. At a solvent composition of 1:0.5:1.5, the structure of the micelles shifts toward the formation of globular aggregates, but these are still of larger dimension than those in 1:2 ChCl/Gly. Interestingly, both surfactants form elongated aggregates compared to those formed in water where SDS and C_{16}TAB form globular micelles ($r_{po,SDS} \sim 23$ Å, $r_{po,C16TAB} \sim 37$ Å).[68,69] Furthermore, the strong peak which appears as a result of intermicellar interactions in water vanishes in DES at these concentrations, suggesting that long-range electrostatic interactions disappear as a result of the low permittivity of the solvent compared to water.[70]

Structure of Interacting Micelles at Higher Surfactant Concentrations. At higher surfactant concentrations (130 mM), intermicellar interactions begin to affect the scattering pattern; thus, the structure factor must be considered to correctly extract structural information. In order to determine the structure of interacting micelles, a uniform ellipsoid model was combined with an effective hard sphere structure factor, as introduced in the Data Analysis section. Figure 3 shows the SANS data of SDS, C_{12}TAB, and C_{16}TAB at 130 mM in the DES with different hydrogen bond donor compositions in the isotopic mixture of deuterated surfactant in protiated solvent. The results from these fits are also included in Figure 3. The error bars seen in the data are the result of averaging the values obtained from fits to the data of multiple contrasts of the same mixture. A full record of the fitting parameters is presented in the Supporting Information.

The structural transitions in micelles observed in the dilute regime also occur at higher concentrations, where the structure factor contribution begins to alter the experimental scattering signal. While little variation is observed in the cross section of the micelles (r_{eq}), a change in elongation (r_{po}) is seen with varying solvent composition. The cross section of the micelles is similar for those formed by the C_{12} surfactants, SDS, and C_{12}TAB, and these are smaller than those of C_{16}TAB, consistent with previous observations and the results obtained for micellization in water.[68,69] Fitted values for the equatorial radius are slightly lower than the extended tail lengths calculated for the surfactants (Table S3), suggesting slight coiling of the surfactant tails within micelles; however, for high degrees of elongation (low glycerol content), the extended tail length value lies within the error calculated for the equatorial radii.

As observed at lower concentrations, varying the urea/glycerol ratio in the DES gave rise to SDS micelles with degrees of elongation varying between the values seen for ChCl/U and ChCl/Gly.[31,35] In ChCl/U, SDS forms highly elongated micelles with aspect ratios between 8.8 and 13.5, whereas in ChCl/Gly, globular micelles are formed with aspect ratios of around 2. Predictably, varying the urea/glycerol ratio in the DES gave rise to micelles with degrees of elongation which lie between these two extremes. An increase in the glycerol content in the solvent leads to the formation of shorter micelles, and this is also observed for the C_nTAB surfactants. Again, remarkable differences in the extent of elongation are observed for C_{16}TAB micelles as these go from elongated

https://dx.doi.org/10.1021/acs.jpcb.0c03876
J. Phys. Chem. B 2020, 124, 6004−6014

aggregates at low glycerol content to globular micelles at high glycerol content. However, it was unfortunately not possible to obtain a similar comparison in both binary DES for C_nTAB surfactants due to their insolubility in ChCl/U. The structural transition of C_{12}TAB micelles is less pronounced, but although changes in r_{po} are within the error, the same trend reported for SDS and C_{16}TAB is observed for C_{12}TAB.

An interesting observation may be made when looking at the trends in the micelle volume fraction ($\Phi_{P(q)}$) and effective volume fraction ($\Phi_{S(q)}$). The volume fraction of micelles shows small variations between solvents. These variations may be potentially attributed to changes in the monomer solubility (CMC) or small differences in sample concentration, but those changes seem to be minor.[32] However, the changes in the effective volume fraction seem to follow a clear increasing trend for all of the surfactants at higher glycerol contents and are consistently higher than the fitted values of micelle volume fraction. The observation that the effective volume fraction is larger than the bare micelle volume fraction has been previously reported and attributed to short-range electrostatic repulsion occurring between charged micelles in DES, which results in a larger effective excluded volume than that physically occupied by the micelles.[31] Furthermore, this effective interaction was additionally reported to be higher between micelles with a shorter tail length (e.g., compare $\Phi_{S(q),C_{12}TAB} > \Phi_{S(q),C_{16}TAB}$ at similar micelle volume fraction).[31] This effect may result from a lower counterion condensation on C_{12} micelles, also resulting in shorter aggregates than seen for its C_{16} analogue, as has also been previously observed in water.[71] Comparing the intermicellar interactions in these systems to other micellar systems in DES, the interactions were found to be higher than those observed in carboxylic acid containing deep eutectic solvents, such as choline chloride/malonic acid, where the presence of the acid is thought to provide a greater charge screening effect,[50] but they were comparable to those observed for micelles in ChCl/Gly.[31] Charge screening observed in the carboxylic acid based DES also resulted in the formation of longer micelles in that system due to the reduction in effective headgroup area.

Solvation and Counterion Condensation. Variation of micelle shape in different solvents for the same surfactant depends largely on changes in the apparent headgroup area, assuming that the solvent does not penetrate into the micelle core. Therefore, understanding the condensation of counterions and the monomer−monomer interactions at the micelle interface becomes important in order to understand the process of micellization and micelle structure.

In addition to a uniform ellipsoid model, an attempt to determine the cross-sectional structure of the micelles was performed through the co-refinement of several neutron contrasts (represented schematically in Figure S5), which resulted in a model of the solvation mechanism for SDS and C_{16}TAB micelles in ChCl/U/Gly DES. These data were fitted to a core−shell model which contains fitting parameters of equatorial radius of the core, r_{eq}, the polar radius of the core, r_{po}, and the shell thickness, T_{shell}. The ratio of shell thickness between polar and equatorial axis was fixed to 1. The SLD of the core was fixed as the surfactant tail SLD, while the SLD of the shell was fitted to assess solvent penetration into the micelle. The SDS data were simultaneously fitted for three contrasts: SDS-d_{25} in h-ChCl/h-U/h-Gly, h-SDS in d-ChCl/d-U/d-Gly, and SDS-d_{25} in h-ChCl/d-U/d-Gly, whereas the C_{16}TAB data were simultaneously fitted for C_{16}TAB-d_{42} in h-ChCl/h-U/h-Gly and h-C_{16}TAB in d-ChCl/d-U/d-Gly.

For SDS, the equatorial radius of the core ($r_{eq,core}$) was fixed to the value 14.5 Å, which was previously obtained through the refinement of SAXS and SANS data of SDS in 1:2 ChCl/U.[30] The thickness of the shell (T_{shell}) was allowed to vary between 3 and 12 Å, and the shell SLD between those values of protiated and deuterated solvent. For C_{16}TAB, the shell thickness in each case was allowed to vary from 4−10 Å,[31] while both the polar and equatorial radii were fitted. The main results from the simultaneous fit of all SDS and C_{16}TAB contrasts are presented in Tables 2 and 3, respectively. The plots with the data and best fits from the core−shell ellipsoid modeling are presented in Figure S6.

Table 2. Parameters for the Best Fit of 25 mM SDS in ChCl/U at Different Hydrogen Bond Donor Mole Ratios[a]

DES ratio	$r_{eq,core}$/Å	$r_{po,core}$/Å	T_{shell}/Å	SLD_{shell}/× 10^{-6} Å^{-2}
1:1.5:0.5	14.5 ± 0.5	61.6 ± 0.4	5.7 ± 1.2	(1) 1.7 ± 0.2, (2) 5.4 ± 0.2, (3) 4.7 ± 0.2
1:1:1	14.5 ± 0.5	54.1 ± 0.2	5.1 ± 0.7	(1) 2.5 ± 0.4, (2) 5.2 ± 0.4, (3) 4.8 ± 0.7
1:0.5:1.5	14.5 ± 0.5	39.9 ± 0.4	4.7 ± 1.7	(1) 2.9 ± 0.8, (2) 4.9 ± 0.7, (3) 4.8 ± 1.4

[a]The SLD_{shell} for each contrast is reported as follows: (1) SDS-d_{25} in h-ChCl/h-U/h-Gly, (2) h-SDS in d-ChCl/d-U/d-Gly, and (3) SDS-d_{25} in h-ChCl/d-U/d-Gly. The errors result from the simultaneous fits of the three contrasts.

Table 3. Parameters for the Best Fit of 130 mM C_{16}TAB in ChCl/U/Gly at Different Hydrogen Bond Donor Mole Ratios[a]

DES ratio	$r_{eq,core}$/Å	$r_{po,core}$/Å	T_{shell}/ Å	SLD_{shell}/x10^{-6} Å^{-2}
1:1.5:0.5	17.5 ± 0.5	138.2 ± 2.5	4.6 ± 0.5	(1) 7.1 ± 0.2, (2) 0.18 ± 0.3
1:1:1	16.2 ± 0.8	111.8 ± 2	4.5 ± 0.3	(1) 7.0 ± 0.4, (2) 0.2 ± 0.2
1:0.5:1.5	16.4 ± 0.7	50.8 ± 1.6	4.7 ± 0.3	(1) 6.34 ± 0.3, (2) 1.3 ± 0.2

[a]The SLD_{shell} for each contrast is reported as follows: (1) C_{16}TAB-d_{42} in h-ChCl/h-U/h-Gly, (2) h-C_{16}TAB in d-ChCl/d-U/d-Gly.

Consistent with the results obtained through the uniform ellipsoid modeling, the elongation of the micelles decreases with increasing glycerol content in the DES. Importantly, a change in the SLD of the shell region is observed with varying solvent composition. The isotopic mixtures (1) and (2), where full contrast exists between micelle and the solvent, gives information on the degree of solvation. For the case of SDS, comparing those SLD values with the SLD of the sulfate group (SLD_{SO_4} = 4.57 × 10^{-6} Å^{-2}), an increased degree of solvation is observed at lower glycerol contents as the headgroup SLD is reduced in protiated solvent and increased in the deuterated solvent. When observing changes in the partial mixture (3), a small increase in the SLD is observed. As the deuterated components (high SLD) in the partial mixture are the hydrogen bond donors, a qualitative interpretation is that there exists a preferential solvation by those compounds. Although it is difficult to draw a detailed solvation mechanism due to the limited contrast information, these results indicate

https://dx.doi.org/10.1021/acs.jpcb.0c03876
J. Phys. Chem. B 2020, 124, 6004−6014

that the solvation in this system relies on the segregation of solvent components around the micellar environment, where an excess of the hydrogen bond donors (either together or also segregated) preferentially sit around the micelle headgroup. In contrast, for C_{16}TAB, the apparent headgroup region thickness and SLD are roughly constant for the lower glycerol content DES. The SLD values are close to those expected for perdeuterated (7.12×10^{-6} Å^{-2}) and protiated (0.18×10^{-6} Å^{-2}) quaternary ammonium headgroups, and the shell thickness is close to the dimensions of this group, suggesting that little solvent penetration into the shell occurs. A higher degree of solvent penetration into the headgroup region occurs in the DES with the highest glycerol content.

The degree of elongation observed for micelles may be directly linked to interaction of the solvent with the surfactant headgroup and the interaction of the counterion with the solvent. Several observations serve as evidence for this dependence. It has been shown for both aqueous[72] and DES surfactant solutions[32] that a variation in the counterion can influence the solubility of the surfactant molecule, and so the CMC. A lower CMC is reported for mixtures where the surfactant counterion interacts strongly with the headgroup, usually described as a "salting out" effect.[73,74] Furthermore, in DES, varying the counterion on SDS micelles resulted in a change in the value of the semi-major axis of the micelles,[32] implying that different counterions bind to the micelle surface to a different extent, similar to observations in water. The CMC of anionic surfactants has been found to be much lower in DES than that in aqueous solutions, which may be attributed to the relatively poor solubility of the surfactant molecules in the DES as compared to water, suggested to be caused by the binding of the cholinium ion to the anionic headgroups.[30,32] This assumption appears to contradict the results from fitting of the shell region above, which suggests that the sulfate headgroup is preferentially solvated by the hydrogen bond donors in these solutions. However, the thickness of the headgroup region is substantially larger than the sulfate group alone, allowing for the possibility that a cholinium ion may be present in this layer in addition to the hydrogen bond donors. Since the headgroup solvation increases with increased amounts of urea in the solvent it may be that the smaller H-bond donor molecule can solvate the sulfate−cholinium ion pair more efficiently than the glycerol but without further detailed contrast information this cannot be confirmed. Conversely, the CMCs of C_nTAB surfactants dissolved in ChCl/glycerol were found to be higher than those in water,[31] as is normally found for surfactants in less polar media.[75,76] These differences, even with identical surfactant tails, indicates the interaction of the surfactant headgroup and counterion with the solvent is key to explaining this behavior.

In order to rationalize the composition dependence of the micelle morphology which we have observed, it is necessary to consider two factors: charge screening in the system and the solubility of the counterions in the DES. It has been noted that the micelle morphology of surfactant molecules in water can be altered by the addition of salt. This is attributed to counterion condensation on the micelles which screens the charge on the headgroup, reducing the apparent headgroup area allowing elongated structures to form. In dilute salt solutions, C_nTAB surfactants have been reported to form spherical micelles,[77] but it has been found that at moderate to high salt concentrations, these micelles transition from globular to rodlike structures.[78,79] Such an observation may be explained by the fact that the salt provides a charge-screening effect on the micelle surface and neutralizes the charges in the solvent to a degree. These charge-screened micelles exhibit weaker Coulomb interactions between headgroups, causing micelle growth in a lateral direction with little increase in their semi-minor axis. As such, micelle elongation in these solvents could be due to the presence of the choline chloride salt within the DES, providing ions which screen charges on the surfactant molecules.

Second, the solubility of small ions in the investigated DES must be considered. The solubilities of NaBr (a salt comprising both the SDS and C_nTAB counterions) in the DES with urea/glycerol ratios of 1.5:0.5, 1:1, and 0.5:1.5 were measured and are estimated to be 50, 58, and 65 g kg^{-1}, respectively. The solubility of NaBr in glycerol is 387 g kg^{-1}, and in water it is approximately 943 g kg^{-1}.[57,80] By contrast, our determined values for the DES are lower, with a higher glycerol content DES showing increased NaBr solubility. From this, it can be inferred that the low solubility of these inorganic cations in the DES results in a tighter binding of the surfactant counterion (Na^+ or Br^-) to the micelle surface, resulting in increased micelle elongation. Stronger counterion binding to the sulfate headgroup in SDS may also allow rationalization of the enhanced presence of the hydrogen bond donors in the micelle headgroup region suggested by the SANS fitting above. Increased binding of the Na^+ counterion would lower the observed CMC in these solvents, so specific binding of the cholinium ion may not be necessary to explain this effect.

CONCLUSIONS

The effect of solvent composition in a ternary DES on the micellization of cationic and anionic surfactants has been investigated. A set of hybrid DES were prepared in ratios of 1:1.5:0.5, 1:1:1, and 1:0.5:1.5 choline chloride/urea/glycerol. Preliminary studies on the properties of the ternary DES show little variation between them in surface tension, density, viscosity, or Gordon parameter. However, previous investigations showed that surfactant behavior in choline chloride/urea differs significantly from that in choline chloride/glycerol, and as such, the micellization in these mixed environments could be used to tune morphologies between those two extremes. The morphology of SDS, C_{12}TAB, and C_{16}TAB micelles were investigated using contrast variation small-angle neutron scattering. The results presented here show that the formation of these mixed solvents does indeed enable the modulation of micelle morphology, transitioning from elongated micelles at low glycerol content to globular aggregates at higher glycerol contents. Interestingly, these mixtures allow the solubilization of the otherwise insoluble cationic surfactants C_{12}TAB and C_{16}TAB in urea-based DES, which also resulted in the formation of micelles with different structural features. There is a strong suggestion that the elongation of the micelles is a direct result of headgroup solvation and counterion binding to the surface. While the SDS headgroup is solvated by the hydrogen bond donor species at all solvent compositions, the cationic surfactants only show significant solvent−headgroup interactions at the highest glycerol content. Measurements of the solubility of NaBr in the DES show that it is markedly lower than in water or glycerol, with a slight variation across the three solvent compositions according to the glycerol content. The solvents with the lowest counterion solubility likely result in higher counterion binding to the micelles, neutralizing headgroup

https://dx.doi.org/10.1021/acs.jpcb.0c03876
J. Phys. Chem. B 2020, 124, 6004−6014

charges and allowing elongation of the micelles. The results of this study have provided further insight into the mechanism of micelle formation in the DES and the factors that are vital to understand in order to achieve controlled self-assembly in these unique solvents.

■ ASSOCIATED CONTENT

Supporting Information

The Supporting Information is available free of charge at https://pubs.acs.org/doi/10.1021/acs.jpcb.0c03876.

Characterization data for the ternary DES (DSC, viscosity with temperature, and glass transition temperatures calculated from viscosity); scattering length densities for the ternary DES, their components, and surfactant components used to fit SANS data; model fitting trials; details of parameters from SANS fitting and diagrams showing a prolate ellipsoid and a representation of the contrast variation technique in neutron scattering (PDF)

■ AUTHOR INFORMATION

Corresponding Author

Karen J. Edler − *Department of Chemistry, University of Bath, Bath BA2 7AY, United Kingdom;* orcid.org/0000-0001-5822-0127; Phone: +441225 384192; Email: k.edler@bath.ac.uk

Authors

Ria S. Atri − *EPSRC Centre for Doctoral Training in Sustainable Chemical Technologies and Department of Chemistry, University of Bath, Bath BA2 7AY, United Kingdom;* orcid.org/0000-0002-9439-8982

Adrian Sanchez-Fernandez − *Department of Chemistry, University of Bath, Bath BA2 7AY, United Kingdom; Food Technology, Engineering and Nutrition, Lund University, 221 00 Lund, Sweden;* orcid.org/0000-0002-0241-1191

Oliver S. Hammond − *EPSRC Centre for Doctoral Training in Sustainable Chemical Technologies and Department of Chemistry, University of Bath, Bath BA2 7AY, United Kingdom; Laboratoire de Chimie, École Normale Supérieure de Lyon, Lyon 69007, France;* orcid.org/0000-0002-5612-9343

Iva Manasi − *Department of Chemistry, University of Bath, Bath BA2 7AY, United Kingdom*

James Doutch − *ISIS Neutron and Muon Source, Science & Technology Facilities Council, Rutherford Appleton Laboratory, Didcot OX11 0QX, United Kingdom*

James P. Tellam − *ISIS Neutron and Muon Source, Science & Technology Facilities Council, Rutherford Appleton Laboratory, Didcot OX11 0QX, United Kingdom*

Complete contact information is available at: https://pubs.acs.org/10.1021/acs.jpcb.0c03876

Notes

The authors declare no competing financial interest.

ISIS Neutron and Muon Source experiment numbers are RB1720289 (DOI: 10.5286/ISIS.E.RB1720289) and RB1910484 (DOI: 10.5286/ISIS.E.RB1910484). All data created as part of the research for this publication are openly available from the University of Bath data archive at DOI: 10.15125/BATH-00860.

■ ACKNOWLEDGMENTS

R.A. and O.S.H acknowledge funding from the EPSRC Centre for Doctoral Training in Sustainable Chemical Technologies, EPSRC Grant EP/L016354/1. O.S.H. further acknowledges funding from ISIS Neutron and Muon Source (STFC Studentship Agreement 3578). A.S.F was funded by the European Spallation Source and the University of Bath Alumni Fund. I.M. thanks the EPSRC for funding (Grant No. EP/S020772/1). We thank the ISIS Neutron and Muon Source for awarded beamtime. R.A. thanks Dr. Martin Levere from the Materials and Chemical Characterisation (MC^2) facility at the University of Bath for assistance with DSC measurements. This work benefited from the use of the SasView application, originally developed under NSF award DMR-0520547. SasView contains code developed with funding from the European Union's Horizon 2020 research and innovation programme under the SINE2020 project, Grant No. 654000.

■ REFERENCES

(1) Evans, D. F.; Yamauchi, A.; Roman, R.; Casassa, E. Z. Micelle formation in ethylammonium nitrate, a low-melting fused salt. *J. Colloid Interface Sci.* **1982**, *88*, 89−96.

(2) Greaves, T. L.; Drummond, C. J. Ionic liquids as amphiphile self-assembly media. *Chem. Soc. Rev.* **2008**, *37*, 1709.

(3) Lu, J.; Yan, F.; Texter, J. Advanced applications of ionic liquids in polymer science. *Prog. Polym. Sci.* **2009**, *34*, 431−448.

(4) Mohshim, D. F.; Mukhtar, H.; Man, Z. Ionic liquid polymeric membrane: Synthesis, characterization & performance evaluation. *Key Eng. Mater.* **2013**, *594*−*595*, 18−23.

(5) Rynkowska, E.; Fatyeyeva, K.; Kujawski, W. Application of polymer-based membranes containing ionic liquids in membrane separation processes: a critical review. *Rev. Chem. Eng.* **2018**, *34*, 341−363.

(6) Mohamed Isa, E. D.; Abdul Rahman, M. B.; Ahmad, H. Monodispersed mesoporous silica nanospheres based on pyridinium ionic liquids. *J. Porous Mater.* **2018**, *25*, 1439−1446.

(7) Rameli, N.; Jumbri, K.; Wahab, R. A.; Ramli, A.; Huyop, F. Synthesis and characterization of mesoporous silica nanoparticles using ionic liquids as a template. *J. Phys.: Conf. Ser.* **2018**, *1123*, 012068.

(8) Dutta, R.; Kundu, S.; Sarkar, N. Ionic liquid-induced aggregate formation and their applications. *Biophys. Rev.* **2018**, *10*, 861−871.

(9) Maugeri, Z.; Domínguez De María, P. Novel choline-chloride-based deep-eutectic-solvents with renewable hydrogen bond donors: levulinic acid and sugar-based polyols. *RSC Adv.* **2012**, *2*, 421.

(10) Ge, X.; Gu, C.; Wang, X.; Tu, J. Deep eutectic solvents (DESs)-derived advanced functional materials for energy and environmental applications: challenges, opportunities, and future vision. *J. Mater. Chem. A* **2017**, *5*, 8209−8229.

(11) Rodríguez-Álvarez, M. J.; García-Álvarez, J.; Uzelac, M.; Fairley, M.; O'Hara, C. T.; Hevia, E. Introducing glycerol as a sustainable solvent to organolithium chemistry: Ultrafast chemoselective addition of aryllithium reagents to nitriles under air and at ambient temperature. *Chem. - Eur. J.* **2018**, *24*, 1720−1725.

(12) Lü, H.; Li, P.; Liu, Y.; Hao, L.; Ren, W.; Zhu, W.; Deng, C.; Yang, F. Synthesis of a hybrid Anderson-type polyoxometalate in deep eutectic solvents (DESs) for deep desulphurization of model diesel in ionic liquids (ILs). *Chem. Eng. J.* **2017**, *313*, 1004−1009.

(13) Parnham, E. R.; Morris, R. E. Ionothermal synthesis of zeolites, metal-organic frameworks, and inorganic-organic hybrids. *Acc. Chem. Res.* **2007**, *40*, 1005−1013.

(14) Yang, C.; Gao, M. Y.; Zhang, Q. B.; Zeng, J. R.; Li, X. T.; Abbott, A. P. In-situ activation of self-supported 3D hierarchically porous Ni_3S_2 films grown on nanoporous copper as excellent pH-universal electrocatalysts for hydrogen evolution reaction. *Nano Energy* **2017**, *36*, 85−94.

(15) Wagle, D. V.; Zhao, H.; Baker, G. A. Deep eutectic solvents: Sustainable media for nanoscale and functional materials. *Acc. Chem. Res.* **2014**, *47*, 2299−2308.
(16) Dai, Y.; Witkamp, G.-J.; Verpoorte, R.; Choi, Y. H. Tailoring properties of natural deep eutectic solvents with water to facilitate their applications. *Food Chem.* **2015**, *187*, 14−19.
(17) Albler, F. J.; Bica, K.; Foreman, M. R. S. J.; Holgersson, S.; Tyumentsev, M. S. A comparison of two methods of recovering cobalt from a deep eutectic solvent: Implications for battery recycling. *J. Cleaner Prod.* **2017**, *167*, 806−814.
(18) Ceblin, M. U.; Zeller, S.; Schick, B.; Kibler, L. A.; Jacob, T. Electrodeposition of Ag onto Au(111) from deep eutectic solvents. *ChemElectroChem* **2019**, *6*, 141−146.
(19) Abbott, A. P.; El Ttaib, K.; Frisch, G.; McKenzie, K. J.; Ryder, K. S. Electrodeposition of copper composites from deep eutectic solvents based on choline chloride. *Phys. Chem. Chem. Phys.* **2009**, *11*, 4269.
(20) Sebastián, P.; Vallés, E.; Gómez, E. First stages of silver electrodeposition in a deep eutectic solvent. Comparative behavior in aqueous medium. *Electrochim. Acta* **2013**, *112*, 149−158.
(21) Bryant, S. J.; Atkin, R.; Warr, G. G. Spontaneous vesicle formation in a deep eutectic solvent. *Soft Matter* **2016**, *12*, 1645−1648.
(22) Bryant, S. J.; Atkin, R.; Warr, G. G. Effect of deep eutectic solvent nanostructure on phospholipid bilayer phases. *Langmuir* **2017**, *33*, 6878−6884.
(23) Chen, Z.; McDonald, S.; FitzGerald, P.; Warr, G. G.; Atkin, R. Small angle neutron scattering study of the conformation of poly(ethylene oxide) dissolved in deep eutectic solvents. *J. Colloid Interface Sci.* **2017**, *506*, 486−492.
(24) Chen, Y.; Mu, T. Application of deep eutectic solvents in biomass pretreatment and conversion. *Green Energy Environ.* **2019**, *4*, 95−115.
(25) Sapir, L.; Stanley, C. B.; Harries, D. Properties of polyvinylpyrrolidone in a deep eutectic solvent. *J. Phys. Chem. A* **2016**, *120*, 3253−3259.
(26) Sanchez-Fernandez, A.; Edler, K. J.; Arnold, T.; Alba Venero, D.; Jackson, A. J. Protein conformation in pure and hydrated deep eutectic solvents. *Phys. Chem. Chem. Phys.* **2017**, *19*, 8667−8670.
(27) Lee, M. S.; Lee, K.; Nam, M. W.; Jeong, K. M.; Lee, J. E.; Kim, N. W.; Yin, Y.; Lim, S. Y.; Yoo, D. E.; Lee, J.; et al. Natural deep eutectic solvents as a storage medium for human interferon-α2: a green and improved strategy for room-temperature biologics. *J. Ind. Eng. Chem.* **2018**, *65*, 343−348.
(28) Xu, K.; Xu, P.; Wang, Y. Aqueous biphasic systems formed by hydrophilic and hydrophobic deep eutectic solvents for the partitioning of dyes. *Talanta* **2020**, *213*, 120839.
(29) Pal, M.; Yadav, A.; Pandey, S. Aggregation of carbocyanine dyes in choline chloride-based deep eutectic solvents in the presence of an aqueous base. *Langmuir* **2017**, *33*, 9781−9792.
(30) Arnold, T.; Jackson, A. J.; Sanchez-Fernandez, A.; Magnone, D.; Terry, A. E.; Edler, K. J. Surfactant behavior of sodium dodecylsulfate in deep eutectic solvent choline chloride/urea. *Langmuir* **2015**, *31*, 12894−12902.
(31) Sanchez-Fernandez, A.; Arnold, T.; Jackson, A. J.; Fussell, S. L.; Heenan, R. K.; Campbell, R. A.; Edler, K. J. Micellization of alkyltrimethylammonium bromide surfactants in choline chloride:glycerol deep eutectic solvent. *Phys. Chem. Chem. Phys.* **2016**, *18*, 33240−33249.
(32) Sanchez-Fernandez, A.; Hammond, O. S.; Edler, K. J.; Arnold, T.; Doutch, J.; Dalgliesh, R. M.; Li, P.; Ma, K.; Jackson, A. J. Counterion binding alters surfactant self-assembly in deep eutectic solvents. *Phys. Chem. Chem. Phys.* **2018**, *20*, 13952−13961.
(33) Dolan, A.; Atkin, R.; Warr, G. G. The origin of surfactant amphiphilicity and self-assembly in protic ionic liquids. *Chem. Sci.* **2015**, *6*, 6189−6198.
(34) Fuguet, E.; Ràfols, C.; Rosés, M. Characterization of the solvation properties of surfactants by solvatochromic indicators. *Langmuir* **2003**, *19*, 6685−6692.
(35) Sanchez-Fernandez, A.; Edler, K. J.; Arnold, T.; Heenan, R. K.; Porcar, L.; Terrill, N. J.; Terry, A. E.; Jackson, A. J. Micelle structure in a deep eutectic solvent: a small-angle scattering study. *Phys. Chem. Chem. Phys.* **2016**, *18*, 14063−14073.
(36) Berr, S.; Jones, R. R. M.; Johnson, J. S. Effect of counterion on the size and charge of alkyltrimethylammonium halide micelles as a function of chain length and concentration as determined by small-angle neutron scattering. *J. Phys. Chem.* **1992**, *96*, 5611−5614.
(37) Han, L.; Che, S. Anionic surfactant templated mesoporous silicas (AMSs). *Chem. Soc. Rev.* **2013**, *42*, 3740−3752.
(38) Gai, F.; Zhou, T.; Chu, G.; Li, Y.; Liu, Y.; Huo, Q.; Akhtar, F. Mixed anionic surfactant-templated mesoporous silica nanoparticles for fluorescence detection of Fe^{3+}. *Dalt. Trans.* **2016**, *45*, 508−514.
(39) Luo, H.; Lin, Q.; Baber, S.; Naalla, M. Surfactant-templated mesoporous metal oxide nanowires. *J. Nanomater.* **2010**, *2010*, 1−6.
(40) Hu, L.; Yan, Z.; Zhang, J.; Peng, X.; Mo, X.; Wang, A.; Chen, L. Surfactant aggregates within deep eutectic solvent-assisted synthesis of hierarchical ZIF-8 with tunable porosity and enhanced catalytic activity. *J. Mater. Sci.* **2019**, *54*, 11009−11023.
(41) Hammond, O. S.; Eslava, S.; Smith, A. J.; Zhang, J.; Edler, K. J. Microwave-assisted deep eutectic-solvothermal preparation of iron oxide nanoparticles for photoelectrochemical solar water splitting. *J. Mater. Chem. A* **2017**, *5*, 16189−16199.
(42) Kadhom, M. A.; Abdullah, G. H.; Al-Bayati, N. Studying two series of ternary deep eutectic solvents (choline chloride-urea-glycerol) and (choline chloride-malic acid-glycerol), synthesis and characterizations. *Arabian J. Sci. Eng.* **2017**, *42*, 1579−1589.
(43) Heenan, R. K.; Penfold, J.; King, S. M. SANS at pulsed neutron sources: Present and future prospects. *J. Appl. Crystallogr.* **1997**, *30*, 1140−1147.
(44) Simeonov, S. P.; Afonso, C. A. M. Basicity and stability of urea deep eutectic mixtures. *RSC Adv.* **2016**, *6*, 5485−5490.
(45) Arnold, O.; Bilheux, J. C.; Borreguero, J. M.; Buts, A.; Campbell, S. I.; Chapon, L.; Doucet, M.; Draper, N.; Ferraz Leal, R.; Gigg, M. A.; et al. Mantid—Data analysis and visualization package for neutron scattering and μ SR experiments. *Nucl. Instrum. Methods Phys. Res., Sect. A* **2014**, *764*, 156−166.
(46) Kline, S. R. Reduction and analysis of SANS and USANS data using IGOR Pro. *J. Appl. Crystallogr.* **2006**, *39*, 895−900.
(47) Guinier, A.; Fournet, G. *Small-Angle Scattering of X-rays*; Wiley: New York, 1955.
(48) Pedersen, J. S. Analysis of small-angle scattering data from colloids and polymer solutions: Modeling and least-squares fitting. *Adv. Colloid Interface Sci.* **1997**, *70*, 171−210.
(49) Percus, J. K.; Yevick, G. J. Analysis of classical statistical mechanics by means of collective coordinates. *Phys. Rev.* **1958**, *110*, 1−13.
(50) Sanchez-Fernandez, A.; Hammond, O. S.; Jackson, A. J.; Arnold, T.; Doutch, J.; Edler, K. J. Surfactant-solvent interaction effects on the micellization of cationic surfactants in a carboxylic acid-based deep eutectic solvent. *Langmuir* **2017**, *33*, 14304−14314.
(51) Evans, D. F. Self-organization of amphiphiles. *Langmuir* **1988**, *4*, 3−12.
(52) Silverstein, K. A. T.; Haymet, A. D. J.; Dill, K. A. A simple model of water and the hydrophobic effect. *J. Am. Chem. Soc.* **1998**, *120*, 3166−3175.
(53) Warr, G. G.; Atkin, R. Solvophobicity and amphiphilic self-assembly in neoteric and nanostructured solvents. *Curr. Opin. Colloid Interface Sci.* **2020**, *45*, 83−96.
(54) Greaves, T. L.; Drummond, C. J. Solvent nanostructure, the solvophobic effect and amphiphile self-assembly in ionic liquids. *Chem. Soc. Rev.* **2013**, *42*, 1096−1120.
(55) Vargaftik, N. B.; Volkov, B. N.; Voljak, L. D. International tables of the surface tension of water. *J. Phys. Chem. Ref. Data* **1983**, *12*, 817−820.
(56) Adamenko, I. I.; Bulavin, L. A.; Ilyin, V.; Zelinsky, S. A.; Moroz, K. O. Anomalous behavior of glycerol-water solutions. *J. Mol. Liq.* **2006**, *127*, 90−92.

https://dx.doi.org/10.1021/acs.jpcb.0c03876
J. Phys. Chem. B 2020, 124, 6004−6014

(57) Seidell, A.; Linke, W. *Solubilities of Inorganic and Metal−Organic Compounds*; American Chemical Society: Washington D.C., 1965; p 831.
(58) Xie, Y.; Dong, H.; Zhang, S.; Lu, X.; Ji, X. Effect of water on the density, viscosity, and CO_2 solubility in choline chloride/urea. *J. Chem. Eng. Data* **2014**, *59*, 3344−3352.
(59) Yadav, A.; Trivedi, S.; Rai, R.; Pandey, S. Densities and dynamic viscosities of (choline chloride+glycerol) deep eutectic solvent and its aqueous mixtures in the temperature range (283.15−363.15)K. *Fluid Phase Equilib.* **2014**, *367*, 135−142.
(60) Leron, R. B.; Wong, D. S. H.; Li, M. H. Densities of a deep eutectic solvent based on choline chloride and glycerol and its aqueous mixtures at elevated pressures. *Fluid Phase Equilib.* **2012**, *335*, 32−38.
(61) Jablonský, M.; Škulcová, A.; Ház, A.; Šima, J.; Majová, V. Long-term isothermal stability of deep eutectic solvents. *BioResources* **2018**, *13*, 7545−7559.
(62) Iqbal, M. J.; Rauf, M. A.; Ijaz, N. Surface tension measurements of glycerol with organic cosolvents. *J. Chem. Eng. Data* **1992**, *37*, 45−47.
(63) Greaves, T. L.; Drummond, C. J. Ionic liquids as amphiphile self-assembly media. *Chem. Soc. Rev.* **2008**, *37*, 1709.
(64) Kijevčanin, M. L.; Živković, E. M.; Djordjević, B. D.; Radović, I. R.; Jovanović, J.; Šerbanović, S. P. Experimental determination and modeling of excess molar volumes, viscosities and refractive indices of the binary systems (pyridine + 1-propanol, + 1,2-propanediol, + 1,3-propanediol, and + glycerol). New UNIFAC-VISCO parameters determination. *J. Chem. Thermodyn.* **2013**, *56*, 49−56.
(65) Rabinovich, V. A.; Khavin, Z. I. *Kratkii Khimicheskii Spravochnik*; Leningrad, 1978.
(66) Hammond, O. S. Plant metabolites as green solvents. MRes thesis, University of Bath, United Kingdom, 2015.
(67) Palazzesi, F.; Calvaresi, M.; Zerbetto, F. A molecular dynamics investigation of structure and dynamics of SDS and SDBS micelles. *Soft Matter* **2011**, *7*, 9148.
(68) Berr, S. S. Solvent isotope effects on alkytrimethylammonium bromide micelles as a function of alkyl chain length. *J. Phys. Chem.* **1987**, *91*, 4760−4765.
(69) Hayter, J. B.; Penfold, J. Determination of micelle structure and charge by neutron small-angle scattering. *Colloid Polym. Sci.* **1983**, *261*, 1022−1030.
(70) Pandey, A.; Rai, R.; Pal, M.; Pandey, S. How polar are choline chloride-based deep eutectic solvents? *Phys. Chem. Chem. Phys.* **2014**, *16*, 1559−1568.
(71) Buckingham, S. A.; Garvey, C. J.; Warr, G. G. Effect of head-group size on micellization and phase behavior in quaternary ammonium surfactant systems. *J. Phys. Chem.* **1993**, *97*, 10236−10244.
(72) Horvath, L.; Mihaljević, B.; Tomašić, V.; Risović, D.; Filipović-Vinceković, N. Counterion binding to ionic micelles: Effects of counterion specificity. *J. Dispersion Sci. Technol.* **2001**, *22*, 221−229.
(73) Pandey, S.; Bagwe, R. P.; Shah, D. O. Effect of counterions on surface and foaming properties of dodecyl sulfate. *J. Colloid Interface Sci.* **2003**, *267*, 160−166.
(74) Berr, S. S.; Coleman, M. J.; Jones, R. R. M.; Johnson, J. S. Small-angle neutron scattering study of the structural effects of substitution of tetramethylammonium for sodium as the counterion in dodecyl sulfate micelles. *J. Phys. Chem.* **1986**, *90*, 6492−6499.
(75) Ruiz, C. C.; Díaz-López, L.; Aguiar, J. Micellization of sodium dodecyl sulfate in glycerol aqueous mixtures. *J. Dispersion Sci. Technol.* **2008**, *29*, 266−273.
(76) Rico, I.; Lattes, A. Formamide, a water substitute. 12. Krafft temperature and micelle formation of ionic surfactants in formamide. *J. Phys. Chem.* **1986**, *90*, 5870−5872.
(77) Naskar, B.; Dan, A.; Ghosh, S.; Aswal, V. K.; Moulik, S. P. Revisiting the self-aggregation behavior of cetyltrimethylammonium bromide in aqueous sodium salt solution with varied anions. *J. Mol. Liq.* **2012**, *170*, 1−10.
(78) Quirion, F.; Magid, L. J. Growth and counterion binding of cetyltrimethylammonium bromide aggregates at 25°C: a neutron and light scattering study. *J. Phys. Chem.* **1986**, *90*, 5435−5441.
(79) Imae, T.; Kamiya, R.; Ikeda, S. Formation of spherical and rod-like micelles of cetyltrimethylammonium bromide in aqueous NaBr solutions. *J. Colloid Interface Sci.* **1985**, *108*, 215−225.
(80) Pinho, S. P.; Macedo, E. A. Solubility of NaCl, NaBr, and KCl in water, methanol, ethanol, and their mixed solvents. *J. Chem. Eng. Data* **2005**, *50*, 29−32.

https://dx.doi.org/10.1021/acs.jpcb.0c03876
J. Phys. Chem. B 2020, 124, 6004−6014